Loss of tafazzin results in decreased myoblast differentiation in C2C12 cells: A myoblast model of Barth syndrome and cardiolipin deficiency

Wenjia Lou[1],[¶], **Christian A. Reynolds**[1],[¶], **Yiran Li**[1], **Jenney Liu**[2], **Maik Hüttemann**[2], **Michael Schlame**[3], **David Stevenson**[4], **Douglas Strathdee**[4], and **Miriam L. Greenberg**[1],[*]

[1]Department of Biological Sciences, Wayne State University, Detroit, Michigan, USA

[2]Center for Molecular Medicine and Genetics, Wayne State University School of Medicine, Detroit, Michigan, USA

[3]Department of Anesthesiology and Cell Biology, New York University School of Medicine, New York, NY, USA

[4]Transgenic Technology Laboratory, Cancer Research UK Beatson Institute, Garscube Estate, Glasgow, United Kingdom

Abstract

Barth syndrome (BTHS) is an X-linked genetic disorder resulting from mutations in the *tafazzin* gene (*TAZ*), which encodes the transacylase that remodels the mitochondrial phospholipid cardiolipin (CL). While most BTHS patients exhibit pronounced skeletal myopathy, the mechanisms linking defective CL remodeling and skeletal myopathy have not been determined. In this study, we constructed a CRISPR-generated stable tafazzin knockout (TAZ-KO) C2C12 myoblast cell line. TAZ-KO cells exhibit mitochondrial deficits consistent with other models of BTHS, including accumulation of monolyso-CL (MLCL), decreased mitochondrial respiratory, and increased mitochondrial ROS production. Additionally, tafazzin-deficiency was associated with impairment of myocyte differentiation. Future studies should determine whether alterations in myogenic determination contribute to the skeletal myopathy observed in BTHS patients. The BTHS myoblast model will enable studies to elucidate mechanisms by which defective CL remodeling interferes with normal myocyte differentiation and skeletal muscle ontogenesis.

Keywords

cardiolipin; tafazzin; Barth syndrome; myotube differentiation

---

[*]Corresponding author: mgreenberg@wayne.edu, Phone: (313) 577-5202, Address: Department of Biological Sciences, 4105 Biological Sciences Building, 5047 Gullen Mall, Detroit, MI 48202.
[¶]These authors contributed equally to this work.

1. Introduction

Cardiolipin (CL) is a dimeric mitochondrial membrane phospholipid with multiple functions that are conserved from yeast to humans [1–11]. Newly synthesized CL undergoes acyl remodeling to produce CL species enriched with unsaturated acyl groups. Deficient CL remodeling causes Barth syndrome (BTHS), a rare X-linked genetic disorder associated with a broad range of clinical manifestations, including cardiomyopathy, skeletal myopathy, neutropenia, and 3-methylglutaconic aciduria [12, 13]. Specifically, BTHS results from mutations in the *tafazzin* gene (*TAZ)* encoding the transacylase responsible for remodeling of CL. Mutations in *TAZ* lead to decreased unsaturated CL species, reduced total CL content, and an accumulation of monolyso-CL (MLCL), an intermediate of the CL remodeling pathway.

Most patients diagnosed with BTHS exhibit pronounced skeletal myopathy, low muscle mass, delayed gross motor development, exercise intolerance, muscle weakness, and focal myofibrillar degeneration [14, 15]. Consistent with decreased mitochondrial function, skeletal muscle O_2 utilization and peak work rate are significantly lower in BTHS patients than control participants [16]. While it is widely accepted that skeletal myopathy associated with BTHS stems from mitochondrial dysfunction, the mechanisms linking defective CL remodeling and skeletal myopathy have not been clearly elucidated and likely extend beyond compromised ATP generation. Myogenic differentiation is largely controlled by myogenic transcription factors and is accompanied by major changes in mitochondrial metabolism [17–20], mitochondrial energy production [20, 21], and mitochondria-mediated activation of apoptotic pathways [22–24]. Given the central role of mitochondria in myogenic differentiation, we hypothesized that mitochondrial defects associated with BTHS might contribute to skeletal myopathy by interfering with normal myocyte differentiation.

To determine the effect of defective CL remodeling on the myogenic determination, we sought to develop a tafazzin-deficient mammalian skeletal myoblast model. The C2C12 cell line was derived from murine skeletal myoblast cells and represents a widely used model for the study of skeletal muscle development [25], skeletal myopathy [26–28], and skeletal muscle differentiation [29–31]. The cells readily proliferate in high-serum conditions, and differentiate and fuse in low-serum conditions. Tafazzin-deficient C2C12 myocytes would provide a metabolic model for which isogenic cells are available as controls, in contrast to currently used BTHS patient-derived lymphoblast cells. Furthermore, they are experimentally easier and cheaper to manipulate than tafazzin-deficient induced pluripotent stem cells (iPSCs) [32].

In this study, we constructed a CRISPR-generated stable tafazzin knockout (TAZ-KO) C2C12 myocyte cell line. The TAZ-KO cell line exhibits an increased MLCL/CL ratio, decreased mitochondrial respiration, increased mitochondrial ROS production, and defective myocyte differentiation. These results indicate that loss of CL remodeling influences myogenic determination and provide a foundation for future studies to explore potential mechanisms by which CL remodeling affects normal myocyte differentiation. Although BTHS is the only known genetic disorder directly linked to CL, aberrant myocyte

differentiation may contribute to the development of skeletal myopathy associated with other mitochondrial diseases.

2. Materials and methods

2.1 Cell line and growth conditions

Wild type C2C12 cell lines were kindly provided by Dr. Steven Cala, Wayne State University. Growth medium consisted of DMEM (Gibco) containing 10% FBS (Hyclone), 2 mM glutamine (Gibco), penicillin, (100 units/ml) and streptomycin (100 μg/ml) (Invitrogen). Cells were grown at 37°C in a humidified incubator with 5% CO_2. C2C12 myoblast differentiation was induced by shifting cells to DMEM medium containing 2% horse serum (Gibco).

2.2 Construction of TAZ-KO C2C12 cell line using CRISPR

A gRNA targeting mouse TAZ exon 3 was identified using the clustered regulatory interspaced short palindromic repeats (CRISPR) design tool at crispr.mit.edu (G2: TCCTAAAACTCCGCCACATC). To express Cas9 and guide RNA in the mouse-derived C2C12 myoblast cells, complementary oligonucleotides containing the gRNA sequence preceded by a G (for expression from the U6 promoter) were cloned into the *Bbs*I site of plasmid pX330 [33] (a gift from Feng Zhang; Massachusetts Institute of Technology, Cambridge, Massachusetts, USA) [Addgene plasmid # 42230]). The sequence was verified using oligonucleotide primer 330/335 (ACTATCATATGCTTACCGTAAC). The plasmid pPGKpurobpa (a gift from Allan Bradley; Wellcome Trust Sanger Institute, Cambridge, UK) was co-transfected to allow selection under puromycin. Cells were transfected with plasmid pX330-TAZ and pPGKpurobpa using Lipofectamine 2000 (Life Technologies, Inc.). Cells were selected in puromycin-containing DMEM with 10% FBS. Cells were then diluted and put into 96-well plates. Single colonies were picked for screening. To screen for insertions or deletions at the target sites, the following oligonucleotide primers flanking mouse Taz exon 3 were used: FOR: CCAACCACCAGTCTTGCATG; REV: ATCCCTGCCTCCAAGACTTC. Wild type genomic DNA generates a product of 547 bp. Clone No. 3 which generated 3 distinct bands were selected for further analysis. PCR products were inserted into a pGEM®-T Easy Vector (Promega) and 16 individual transformants were analyzed by Sanger sequencing (Applied Genetics Technology Center, Wayne State University School of Medicine).

2.3 Mitochondria extraction

Cells were grown to 100% confluency in 150 mm dishes and collected by scraping followed by centrifugation at 800 rpm for 5 min. The cell pellets were washed with cold PBS and suspended in mitochondrial isolation buffer (280 mM sucrose, 0.25 mM EDTA, 20 mM Tris-HCl, pH 7.2). Cells were manually homogenized with a glass homogenizer. Cell debris was removed by centrifugation at 800 rpm for 5 min. Mitochondria were subsequently collected by centrifugation at 11,500 rpm for 10 min

2.4 Determination of CL by mass spectrometry

Transacylation products were quantified by MALDI-TOF mass spectrometry using the method of Sun et al. [34]. Lipid extracts were dissolved in chloroform/methanol (1:1) and mixed 1:1 with matrix solution containing 20 g/L 9-aminoacridine in 2-propanol/acetonitrile (3:2, v/v). An aliquot of 1 μL or less of this mixture was spotted on a target plate. Measurements were performed with a MALDI Micro MX mass spectrometer (Waters) operated in reflectron mode. The pulse voltage was set to 2000 V, the detector voltage was set to 2200 V, and the TLF delay was set to 700 ns. The nitrogen laser (337 nm) was fired at a rate of 5 Hz, and 10 laser shots were acquired per sub-spectrum. The instrument was operated in negative ion mode with a flight tube voltage of 12 kV, a reflectron voltage of 5.2 kV, and a negative anode voltage of 3.5 kV, and calibrated daily. We typically acquired 100 sub-spectra (representing 1000 laser shots) per sample in a mass range from 400 to 2000 Da. Spectra were only acquired if their base-peak-intensity was within 10–95% of the saturation level. Data were analyzed with the MassLynx 4.1 software.

2.5 Immunoblotting

Mitochondrial protein concentration was determined using the DC Protein Assay Kit (BIO-RAD). Cell extract corresponding to 30 μg protein was analyzed by SDS-PAGE on a 10% gel. Immunoblotting was performed using primary antibodies against tafazzin, NDUFB6, and corresponding secondary antibodies conjugated to horseradish peroxidase. Immunoreactivity was visualized using enhanced chemiluminescence (ECL) substrate (Thermo).

2.6 MTT assay

3000 cells were suspended in 100 μL of growth medium and seeded into 96-well plates. Viable cells were measured in triplicate using MTT (Fisher) after 3, 24, and 48 h. In brief, 10 μL of 5 mg/mL MTT was added to each well. The inclusion of an additional set of wells treated with MTT but containing no cells served as a negative control. The plate was incubated for 4 h at 37°C in a culture hood. The medium was carefully removed and 150 μL DMSO was added to dissolve the MTT product. The plate was covered with foil and incubated for 10 min at 37°C. Samples from each well were mixed well with a pipette, and absorbance was read at 570 nm.

2.7 Mitochondrial respiration measurements

The Seahorse Extracellular Flux Analyzer XF^{e}24 (Agilent, Santa Clara, CA) was used to measure oxygen consumption rate (OCR) in WT and TAZ-KO cells. Measurements were taken from intact cells using XF assay medium, pH 7.2, which was supplemented with pyruvate and glucose. Basal OCR was determined for 3 sets of measurements in undifferentiated cells as well as 7-days following a shift to differentiation media. 1 μM oligomycin A, 1 μM FCCP, and 10 μM Rotenone plus 10 μM Antimycin A were added as indicated. Oxygen consumption was normalized to total protein.

2.8 Measurement of mitochondrial membrane potential via TMRM fluorescence

Cells were plated at 40% confluency in 96-well plates in growth medium. After 24 h, the mitochondrial membrane potential was measured using the fluorescent dye Tetramethylrhodamine methyl ester (TMRM) as described previously [35]. Briefly, cells were treated with 150 nM TMRM in growth medium for 30 min at 37°C. The cells were then washed 3 times with PBS, and TMRM fluorescence was measured on a microplate reader (Excitation: 544 nm and Emission: 590 nm). Each assay was performed in parallel with samples containing 10 μM carbonyl-cyanide-4-(trifluoromethoxy)phenylhydrazone (FCCP), which collapses the mitochondrial membrane potential. All data were expressed as the total TMRM fluorescence minus the FCCP treated TMRM fluorescence.

2.9 Measurement of ROS production using MitoSOX

ROS production was measured with MitoSOX™ mitochondrial superoxide indicator (M36008) (Fisher Scientific) following the manufacturer's guide. In brief, the 5 mM MitoSOX™ reagent stock solution was diluted in growth medium to make a 5 μM MitoSOX™ reagent working solution. 1.0 mL of 5 μM MitoSOX™ reagent working solution was applied to cover cells adhering to coverslips. Cells were incubated for 10 min at 37°C, protected from light, then washed gently three times with warm buffer, counterstained with DAPI, and imaged using a Z1 AxioObserver inverted fluorescence microscope equipped with an AxioVision MRm camera (Zeiss). Images were taken using a 20X objective. MitoSOX fluorescence was quantified in all cells within five randomly selected fields of view from three biological replicates using fluorescence density analysis with ZenPro software (Zeiss).

2.10 Immunofluorescence imaging of myotubes

Cells were seeded on gelatin and fibronectin-coated glass coverslips at 40% confluency. Following overnight culture, the growth media containing 10% FBS were replaced with differentiation media containing 2% horse serum. At the indicated times, the cells were fixed with 4% paraformaldehyde. The coverslips were washed three times in buffer (PBS + 0.3% Triton) and then blocked using 10% horse serum (Invitrogen). Coverslips were incubated with primary antibody, mouse anti-MHC (Novus Biologicals; MAB4470), diluted in PBS supplemented with 10% horse serum for 24 h. After washing with PBS, coverslips were incubated with an AlexaFluor 488®-conjugated donkey anti-mouse secondary antibody (1:1000, Jackson ImmunoResearch Laboratories) overnight. Fluorescence microscopy was performed using a Z1 AxioObserver inverted fluorescence microscope equipped with an AxioVision MRm camera (Zeiss) operated by ZenPro software (Zeiss). All images were taken using a 20X objective. Myotube density was quantified using morphometric analysis in five randomly selected fields of view from three biological replicates. MHC-positive myotubes were manually traced, and the myotube density was calculated by dividing the area occupied by MHC-positive myotubes by the total area of the field of view.

2.11 Lactate assay

Lactate production was determined in WT and TAZ-KO cells 7 days after induction of differentiation. Lactate was measured with a kit (Pointe Scientific, Inc. Canton MI) using a

modification to the manufacturer protocol to allow measurement in a 96 well plate and a plate reader. Lactate was measured in triplicate using 2 μL of each sample. A standard curve was generated using dilutions of the lactate standard provided by the manufacturer. Samples were loaded into a 96 well plate, and the kit reagents were added following the manufacturer's directions and incubated at 37°C for 5 mins before reading the absorbance of 550nm. Lactate in the culture medium was then normalized to total protein.

2.12 Statistical Analysis

The results are presented as mean ± S.D. values from at least three biological replicates. Statistical analyses were performed by unpaired Student's t-test. The statistical significance was set at $p < 0.05$.

3. Results

3.1 Construction of a tafazzin knockout C2C12 cell line using CRISPR technology

We generated a TAZ-KO C2C12 myocyte cell line in order to interrogate a potential link between CL remodeling and myocyte differentiation. C2C12 is a well-characterized myoblast cell line that exhibits a high metabolic demand, similar to skeletal muscle cells [25]. These cells proliferate as undifferentiated myoblast cells when grown in media containing high concentrations of serum (10%), and terminally differentiate into multinucleated myotubes when cultured in low serum-containing media. We used the CRISPR approach to generate tafazzin-deficient C2C12 myoblast cells. The pX330-TAZ and pPGKpurobpa plasmids were transfected into C2C12 myoblasts, which were grown in a selective medium. Following serial dilution, cultures derived from single cells were picked, and PCR was used to identify the gene knockout (Fig 1A). Following an initial screen of transfected myoblast cells, we identified 5 knockout strains via PCR. To further confirm genome modifications, we performed a T7 endonuclease assay by mixing equal amounts (100 ng) of both mutant and wild-type reference PCR products which were hybridized via denaturation and annealing. T7 Endonuclease was used to detect mismatches. Using this method, we identified 2 additional knockout strains. Given that the C2C12 cell line is tetraploid with 4 copies of the X chromosomes [36], we selected knockout strain No. 3, in which mutant PCR products differed from the WT reference strain. We then ligated the PCR product into a T-vector, and 16 individual transformants were analyzed by Sanger sequencing. Three different TAZ allele were identified. Allele 1 is a deletion with a G at 298 bp deleted, which leads to a frameshift mutation. Allele 2 has an 83 bp deletion from 243 to 324. Allele 3 has a 133 bp insertion at 298 bp. The WT allele was not detected (Figure 1B). Furthermore, we confirmed the successful knockout by quantifying tafazzin protein level. Tafazzin protein was not detectable via Western blot analysis (Fig 1C).

3.2 Increased MLCL/CL ratio in TAZ-KO cells

The most direct biochemical phenotype associated with tafazzin deficiency is an accumulation of MLCL and a concomitant reduction in CL species containing unsaturated fatty acyl chains. Using MALDI-TOF mass spectrometry, we confirmed that the TAZ-KO C2C12 myoblast cells exhibit reduced tafazzin function, as indicated by the characteristic CL profile of tafazzin deficiency. The MLCL/CL ratio was significantly increased in TAZ-

KO cells compared to controls, and the degree of CL unsaturation was significantly reduced (Fig 2).

3.3 Characterization of tafazzin-deficient C2C12 cells

We measured the proliferative growth of TAZ-KO myoblast cells using the MTT assay to determine if the loss of tafazzin directly affects myoblast proliferation. Deletion of tafazzin did not significantly influence the doubling time of C2C12 cells (Fig 3A). In other BTHS models, including BTHS patient-derived lymphoblast cells and iPSCs, loss of tafazzin results in decreased mitochondrial membrane potential, decreased mitochondrial respiration, and increased mitochondrial ROS production [32, 37]. We assayed these parameters in the TAZ-KO myoblast cells. Assessment of mitochondrial membrane potential using TMRM fluorescence indicated a significant reduction in membrane potential in TAZ-KO myoblasts compared to controls (Fig 3B), which is consistent with other BTHS models [37, 38]. Mitochondrial respiration was measured in intact cells. Basal mitochondrial respiration was significantly affected by tafazzin deficiency in the myoblast cells; however, the maximal respiratory capacity of the TAZ-KO myoblast cells was not significantly decreased compared to controls (Fig 3C–D). This observation contrasts with other BTHS models in which both the basal rate and the maximal rate are decreased by tafazzin deficiency [32, 39]. To quantify mitochondrial ROS production in the myoblast cells, we employed MitoSOX fluorescence staining. Mitochondrial ROS production was significantly increased in TAZ-KO myoblast cells compared to controls (Fig 4).

3.4 CL remodeling is required for myocyte differentiation

C2C12 myoblast cells are routinely used to study skeletal muscle differentiation. These cells grow as undifferentiated myoblasts in growth medium containing 10% fetal bovine serum, and myogenic differentiation can be initiated in cells reaching confluence by shifting the cells to medium containing 2% horse serum [40]. To investigate if myocyte differentiation is affected by the loss of tafazzin, we initiated myogenic differentiation using the widely-used protocol outlined above. As shown by fluorescence microscopy (Fig 5), control myoblast cells morphologically responded to the serum depletion and expressed the skeletal muscle contractile protein myosin heavy chain (MHC). In striking contrast, TAZ-KO myoblast cells exhibited severely impaired phenotypic differentiation into myotubes. Defects in the metabolic transition from glycolysis to mitochondrial oxidative metabolism may contribute to defective myotube differentiation. To determine if the loss of tafazzin alters mitochondrial metabolism associated with myotube differentiation, we measure mitochondrial oxygen consumption rate and lactate production in WT and TAZ-KO C2C12 cells 7-days following the switch to differentiation media. Both basal mitochondrial respiration and maximal respiratory capacity were decreased in TAZ-KO cells (Fig 6A–B). Furthermore, lactate production was significantly increased in TAZ-KO cells (Fig 6C). Taken together, these data indicate that TAZ-KO cells exhibit an increased reliance on glycolysis and decreased flux to mitochondrial oxidative metabolism when compared with WT cells following the switch to myocyte differentiation media.

4. Discussion

Previous studies have utilized tafazzin knockout or BTHS patient-derived iPSCs to generate cardiomyocytes for studying the pathophysiology underlying the cardiomyopathy in BTHS [41–43]. More recently, Lu et al. constructed a tafazzin knockout HEK293 cell line [44]. The TAZ-KO C2C12 cell line generated in the current study represents the first tafazzin-deficient mammalian cell culture model system established in an immortalized skeletal myoblast cell line. Skeletal myopathy associated with BTHS is presumed to result primarily from impaired ATP production owing to alterations in mitochondrial oxidative phosphorylation. In the present study, we provide evidence for an additional link between dysfunctional CL remodeling and disturbed myocyte ontogenesis. Our findings suggest that myocyte differentiation may be affected in BTHS and may contribute to the skeletal myopathy observed in these patients. The current study has generated a new BTHS model for the study of skeletal myopathy. The TAZ-KO C2C12 cells provide an isogenic model system for exploring the muscle-specific effects of tafazzin-deficiency. C2C12 cells are widely used for biochemical and metabolic studies of skeletal myocytes are relatively easy and inexpensive to manipulate. TAZ-KO C2C12 myoblast cells display a mitochondrial phenotype similar to that of BTHS patient tissues and other mammalian models of BTHS. Loss of tafazzin was associated with a significant increase in the MLCL/CL ratio, and a reduction in the number of unsaturated fatty acyl chains incorporated into CL. Furthermore, TAZ-KO myoblast cells display decreased membrane potential, decreased mitochondrial respiratory capacity, and increased mitochondrial ROS production.

Although we found that loss of CL remodeling leads to defective skeletal myocyte differentiation, the mechanism by which myocyte differentiation is affected remains to be elucidated. CL content is an important determinant of mitochondrial membrane structure and cristae density [45], and structural changes resulting from the loss of remodeled CL or from the accumulation of monolyso-CL may physically interfere with regular mitochondrial network fusion status. In BTHS patient-derived lymphoblast cells, mitochondrial hyperproliferation and increased mitochondrial network fragmentation are observed [37, 46]. Currently, little is known regarding the role of mitochondrial network dynamics in controlling cellular differentiation. However, actively dividing blast cells have highly fragmented mitochondrial networks that progressively fuse during terminal differentiation, which is associated with increased respiratory capacity [47]. In general, highly fused mitochondrial networks are associated with maximal respiratory capacity [48–50]. Thus, it is tempting to speculate that loss of tafazzin may interfere with normal differentiation owing to a reduced ability to form highly fused mitochondrial networks. Consistent with this notion, increased mitochondrial network fragmentation and hyperproliferation have been linked to IKK/NF-κB signaling, which partially inhibits myocyte differentiation (34).

What is the relationship between tafazzin deficiency, cellular energy metabolism, and myocyte differentiation? To meet the anabolic demands of proliferation, actively dividing blast cells limit mitochondrial oxidative metabolism to increase cellular biomass via anabolic pathways. Consequently, differentiation requires the induction of mitochondrial oxidative metabolism to support oxidation of glycolysis-derived pyruvate to CO_2. Differentiation is associated with a spectrum of changes in mitochondrial metabolic

machinery, including upregulation of enzymes of the tricarboxylic acid (TCA) cycle and subunits of the mitochondrial respiratory chain, and downregulation of glycolytic enzymes [51–54]. This metabolic transition from glycolysis to mitochondrial oxidative metabolism is necessary for cellular differentiation. Studies of pluripotent stem cell differentiation confirm that inhibition of key glycolytic enzymes promotes differentiation, while impairment of mitochondrial function with respiratory inhibitors improves pluripotency and inhibits differentiation [51, 55]. Accordingly, it is plausible that defective mitochondrial oxidative metabolism contributes to the observed differentiation defect in tafazzin deficient C2C12 myoblast cells.

Given their roles as energy and redox sensors, AMP-activated kinase (AMPK), and the sirtuin family of NAD-dependent deacetylases has been implicated in regulating skeletal muscle differentiation in response to metabolic status [56]. Although very little is known about the role of these proteins in the development of skeletal myopathy, increased AMPK and sirtuin activity have been proposed to inhibit differentiation [57, 58]. It is possible that metabolic and/or redox signaling pathways that regulate myoblast differentiation are affected in tafazzin-deficient cells. Future studies will determine what effect tafazzin deficiency has on cellular metabolism and redox state in order to further elucidate the molecular mechanisms regulating myogenic determination in the TAZ-KO C2C12 cells.

Acknowledgments

Glossary

BTHS	Barth syndrome
CL	cardiolipin
TAZ-KO	tafazzin knockout
MLCL	monolyso-CL

References

1. Joshi AS, Zhou J, Gohil VM, Chen S, Greenberg ML. Cellular functions of cardiolipin in yeast. Biochim Biophys Acta. 2009; 1793:212–218. [PubMed: 18725250]

2. Xu Y, Condell M, Plesken H, Edelman-Novemsky I, Ma J, Ren M, Schlame M. A Drosophila model of Barth syndrome. Proc Natl Acad Sci U S A. 2006; 103:11584–11588. [PubMed: 16855048]

3. Acehan D, Vaz F, Houtkooper RH, James J, Moore V, Tokunaga C, Kulik W, Wansapura J, Toth MJ, Strauss A, Khuchua Z. Cardiac and skeletal muscle defects in a mouse model of human Barth syndrome. J Biol Chem. 2011; 286:899–908. [PubMed: 21068380]

4. Soustek MS, Falk DJ, Mah CS, Toth MJ, Schlame M, Lewin AS, Byrne BJ. Characterization of a transgenic short hairpin RNA-induced murine model of Tafazzin deficiency. Human gene therapy. 2011; 22:865–871. [PubMed: 21091282]

5. Jiang F, Ryan MT, Schlame M, Zhao M, Gu Z, Klingenberg M, Pfanner N, Greenberg ML. Absence of cardiolipin in the crd1 null mutant results in decreased mitochondrial membrane potential and reduced mitochondrial function. J Biol Chem. 2000; 275:22387–22394. [PubMed: 10777514]

6. Koshkin V, Greenberg ML. Oxidative phosphorylation in cardiolipin-lacking yeast mitochondria. Biochem J. 2000; 347(Pt 3):687–691. [PubMed: 10769171]

7. Koshkin V, Greenberg ML. Cardiolipin prevents rate-dependent uncoupling and provides osmotic stability in yeast mitochondria. Biochem J. 2002; 364:317–322. [PubMed: 11988106]

8. McKenzie M, Lazarou M, Thorburn DR, Ryan MT. Mitochondrial respiratory chain supercomplexes are destabilized in Barth Syndrome patients. J Mol Biol. 2006; 361:462–469. [PubMed: 16857210]

9. Pfeiffer K, Gohil V, Stuart RA, Hunte C, Brandt U, Greenberg ML, Schagger H. Cardiolipin stabilizes respiratory chain supercomplexes. J Biol Chem. 2003; 278:52873–52880. [PubMed: 14561769]

10. Chen S, Tarsio M, Kane PM, Greenberg ML. Cardiolipin mediates cross-talk between mitochondria and the vacuole. Mol Biol Cell. 2008; 19:5047–5058. [PubMed: 18799619]

11. Gebert N, Joshi AS, Kutik S, Becker T, McKenzie M, Guan XL, Mooga VP, Stroud DA, Kulkarni G, Wenk MR, Rehling P, Meisinger C, Ryan MT, Wiedemann N, Greenberg ML, Pfanner N. Mitochondrial cardiolipin involved in outer-membrane protein biogenesis: implications for Barth syndrome. Curr Biol. 2009; 19:2133–2139. [PubMed: 19962311]

12. Mazzocco MM, Henry AE, Kelly RI. Barth syndrome is associated with a cognitive phenotype. Journal of developmental and behavioral pediatrics: JDBP. 2007; 28:22. [PubMed: 17353728]

13. Barth PG, Scholte HR, Berden JA, Van der Klei-Van Moorsel JM, Luyt-Houwen IE, Van 't Veer-Korthof ET, Van der Harten JJ, Sobotka-Plojhar MA. An X-linked mitochondrial disease affecting cardiac muscle, skeletal muscle and neutrophil leucocytes. Journal of the neurological sciences. 1983; 62:327–355. [PubMed: 6142097]

14. Barth PG, Wanders RJ, Vreken P, Janssen EA, Lam J, Baas F. X-linked cardioskeletal myopathy and neutropenia (Barth syndrome)(MIM 302060). Journal of inherited metabolic disease. 1999; 22:555–567. [PubMed: 10407787]

15. Spencer CT, Bryant RM, Day J, Gonzalez IL, Colan SD, Thompson WR, Berthy J, Redfearn SP, Byrne BJ. Cardiac and clinical phenotype in Barth syndrome. Pediatrics. 2006; 118:e337–e346. [PubMed: 16847078]

16. Spencer CT, Byrne BJ, Bryant RM, Margossian R, Maisenbacher M, Breitenger P, Benni PB, Redfearn S, Marcus E, Cade WT. Impaired cardiac reserve and severely diminished skeletal muscle O(2) utilization mediate exercise intolerance in Barth syndrome. Am J Physiol Heart Circ Physiol. 2011; 301:H2122–2129. [PubMed: 21873497]

17. Hamai N, Nakamura M, Asano A. Inhibition of mitochondrial protein synthesis impaired C2C12 myoblast differentiation. Cell Struct Funct. 1997; 22:421–431. [PubMed: 9368716]

18. Philp A, Belew MY, Evans A, Pham D, Sivia I, Chen A, Schenk S, Baar K. The PGC-1alpha-related coactivator promotes mitochondrial and myogenic adaptations in C2C12 myotubes. Am J Physiol Regul Integr Comp Physiol. 2011; 301:R864–872. [PubMed: 21795630]

19. Zhu LN, Ren Y, Chen JQ, Wang YZ. Effects of myogenin on muscle fiber types and key metabolic enzymes in gene transfer mice and C2C12 myoblasts. Gene. 2013; 532:246–252. [PubMed: 24055422]

20. Abdel Khalek W, Cortade F, Ollendorff V, Lapasset L, Tintignac L, Chabi B, Wrutniak-Cabello C. SIRT3, a mitochondrial NAD(+)-dependent deacetylase, is involved in the regulation of myoblast differentiation. PLoS One. 2014; 9:e114388. [PubMed: 25489948]

21. Murray J, Huss JM. Estrogen-related receptor alpha regulates skeletal myocyte differentiation via modulation of the ERK MAP kinase pathway. Am J Physiol Cell Physiol. 2011; 301:C630–645. [PubMed: 21562305]

22. Griffiths GS, Doe J, Jijiwa M, Van Ry P, Cruz V, de la Vega M, Ramos JW, Burkin DJ, Matter ML. Bit-1 is an essential regulator of myogenic differentiation. J Cell Sci. 2015; 128:1707–1717. [PubMed: 25770104]

23. Camara Y, Duval C, Sibille B, Villarroya F. Activation of mitochondrial-driven apoptosis in skeletal muscle cells is not mediated by reactive oxygen species production. Int J Biochem Cell Biol. 2007; 39:146–160. [PubMed: 16968671]

24. Ciavarra G, Zacksenhaus E. Multiple pathways counteract cell death induced by RB1 loss: implications for cancer. Cell Cycle. 2011; 10:1533–1539. [PubMed: 21540641]

25. Burattini S, Ferri P, Battistelli M, Curci R, Luchetti F, Falcieri E. C2C12 murine myoblasts as a model of skeletal muscle development: morpho-functional characterization. Eur J Histochem. 2004; 48:223–233. [PubMed: 15596414]

26. Bathe FS, Rommelaere H, Machesky LM. Phenotypes of myopathy-related actin mutants in differentiated C2C12 myotubes. BMC Cell Biol. 2007; 8:2. [PubMed: 17227580]

27. Mullen PJ, Luscher B, Scharnagl H, Krahenbuhl S, Brecht K. Effect of simvastatin on cholesterol metabolism in C2C12 myotubes and HepG2 cells, and consequences for statin-induced myopathy. Biochem Pharmacol. 2010; 79:1200–1209. [PubMed: 20018177]

28. Arya MA, Tai AK, Wooten EC, Parkin CD, Kudryavtseva E, Huggins GS. Notch pathway activation contributes to inhibition of C2C12 myoblast differentiation by ethanol. PLoS One. 2013; 8:e71632. [PubMed: 23977095]

29. Jasmer DP, Kwak D. Fusion and differentiation of murine C2C12 skeletal muscle cells that express Trichinella spiralis p43 protein. Exp Parasitol. 2006; 112:67–75. [PubMed: 16330028]

30. Wallace MA, Della Gatta PA, Ahmad Mir B, Kowalski GM, Kloehn J, McConville MJ, Russell AP, Lamon S. Overexpression of Striated Muscle Activator of Rho Signaling (STARS) Increases C2C12 Skeletal Muscle Cell Differentiation. Front Physiol. 2016; 7:7. [PubMed: 26903873]

31. Ardite E, Barbera JA, Roca J, Fernandez-Checa JC. Glutathione depletion impairs myogenic differentiation of murine skeletal muscle C2C12 cells through sustained NF-kappaB activation. Am J Pathol. 2004; 165:719–728. [PubMed: 15331397]

32. Dudek J, Cheng IF, Balleininger M, Vaz FM, Streckfuss-Bomeke K, Hubscher D, Vukotic M, Wanders RJ, Rehling P, Guan K. Cardiolipin deficiency affects respiratory chain function and organization in an induced pluripotent stem cell model of Barth syndrome. Stem Cell Res. 2013; 11:806–819. [PubMed: 23792436]

33. Cong L, Ran FA, Cox D, Lin S, Barretto R, Habib N, Hsu PD, Wu X, Jiang W, Marraffini LA, Zhang F. Multiplex genome engineering using CRISPR/Cas systems. Science. 2013; 339:819–823. [PubMed: 23287718]

34. Sun G, Yang K, Zhao Z, Guan S, Han X, Gross RW. Matrix-assisted laser desorption/ionization time-of-flight mass spectrometric analysis of cellular glycerophospholipids enabled by multiplexed solvent dependent analyte-matrix interactions. Anal Chem. 2008; 80:7576–7585. [PubMed: 18767869]

35. Brown GC. Nitric oxide and mitochondrial respiration. Biochim Biophys Acta. 1999; 1411:351–369. [PubMed: 10320668]

36. Casas-Delucchi CS, Brero A, Rahn HP, Solovei I, Wutz A, Cremer T, Leonhardt H, Cardoso MC. Histone acetylation controls the inactive X chromosome replication dynamics. Nat Commun. 2011; 2:222. [PubMed: 21364561]

37. Xu Y, Sutachan JJ, Plesken H, Kelley RI, Schlame M. Characterization of lymphoblast mitochondria from patients with Barth syndrome. Lab Invest. 2005; 85:823–830. [PubMed: 15806137]

38. Karkucinska-Wieckowska A, Trubicka J, Werner B, Kokoszynska K, Pajdowska M, Pronicki M, Czarnowska E, Lebiedzinska M, Sykut-Cegielska J, Ziolkowska L, Jaron W, Dobrzanska A, Ciara E, Wieckowski MR, Pronicka E. Left ventricular noncompaction (LVNC) and low mitochondrial membrane potential are specific for Barth syndrome. J Inherit Metab Dis. 2013; 36:929–937. [PubMed: 23361305]

39. Hsu P, Liu X, Zhang J, Wang HG, Ye JM, Shi Y. Cardiolipin remodeling by TAZ/tafazzin is selectively required for the initiation of mitophagy. Autophagy. 2015; 11:643–652. [PubMed: 25919711]

40. Travaglione S, Messina G, Fabbri A, Falzano L, Giammarioli AM, Grossi M, Rufini S, Fiorentini C. Cytotoxic necrotizing factor 1 hinders skeletal muscle differentiation in vitro by perturbing the activation/deactivation balance of Rho GTPases. Cell Death Differ. 2005; 12:78–86. [PubMed: 15514676]

41. Acehan D, Khuchua Z, Houtkooper RH, Malhotra A, Kaufman J, Vaz FM, Ren M, Rockman HA, Stokes DL, Schlame M. Distinct effects of tafazzin deletion in differentiated and undifferentiated mitochondria. Mitochondrion. 2009; 9:86–95. [PubMed: 19114128]

42. Moffat C, Bhatia L, Nguyen T, Lynch P, Wang M, Wang D, Ilkayeva OR, Han X, Hirschey MD, Claypool SM, Seifert EL. Acyl-CoA thioesterase-2 facilitates mitochondrial fatty acid oxidation in the liver. J Lipid Res. 2014; 55:2458–2470. [PubMed: 25114170]

43. Dudek J, Cheng IF, Balleininger M, Vaz FM, Streckfuss-Bömeke K, Hübscher D, Vukotic M, Wanders RJ, Rehling P, Guan K. Cardiolipin deficiency affects respiratory chain function and organization in an induced pluripotent stem cell model of Barth syndrome. Stem cell research. 2013; 11:806–819. [PubMed: 23792436]

44. Lu YW, Galbraith L, Herndon JD, Lu YL, Pras-Raves M, Vervaart M, Van Kampen A, Luyf A, Koehler CM, McCaffery JM, Gottlieb E, Vaz FM, Claypool SM. Defining functional classes of Barth syndrome mutation in humans. Hum Mol Genet. 2016; 25:1754–1770. [PubMed: 26908608]

45. Schlame M. Cardiolipin remodeling and the function of tafazzin. Biochim Biophys Acta. 2013; 1831:582–588. [PubMed: 23200781]

46. Acehan D, Xu Y, Stokes DL, Schlame M. Comparison of lymphoblast mitochondria from normal subjects and patients with Barth syndrome using electron microscopic tomography. Lab Invest. 2007; 87:40–48. [PubMed: 17043667]

47. Zhang JJ. Seamless networks of myocardial bioenergetics. J Physiol. 2011; 589:5013–5014. [PubMed: 22042542]

48. Chen H, Chomyn A, Chan DC. Disruption of fusion results in mitochondrial heterogeneity and dysfunction. The Journal of biological chemistry. 2005; 280:26185–26192. [PubMed: 15899901]

49. Chen H, Detmer SA, Ewald AJ, Griffin EE, Fraser SE, Chan DC. Mitofusins Mfn1 and Mfn2 coordinately regulate mitochondrial fusion and are essential for embryonic development. The Journal of cell biology. 2003; 160:189–200. [PubMed: 12527753]

50. Yu T, Robotham JL, Yoon Y. Increased production of reactive oxygen species in hyperglycemic conditions requires dynamic change of mitochondrial morphology. Proceedings of the National Academy of Sciences of the United States of America. 2006; 103:2653–2658. [PubMed: 16477035]

51. Chung S, Dzeja PP, Faustino RS, Perez-Terzic C, Behfar A, Terzic A. Mitochondrial oxidative metabolism is required for the cardiac differentiation of stem cells. Nat Clin Pract Cardiovasc Med. 2007; 4(Suppl 1):S60–67. [PubMed: 17230217]

52. Armstrong L, Tilgner K, Saretzki G, Atkinson SP, Stojkovic M, Moreno R, Przyborski S, Lako M. Human induced pluripotent stem cell lines show stress defense mechanisms and mitochondrial regulation similar to those of human embryonic stem cells. Stem Cells. 2010; 28:661–673. [PubMed: 20073085]

53. Prigione A, Fauler B, Lurz R, Lehrach H, Adjaye J. The senescence-related mitochondrial/ oxidative stress pathway is repressed in human induced pluripotent stem cells. Stem Cells. 2010; 28:721–733. [PubMed: 20201066]

54. Tormos KV, Anso E, Hamanaka RB, Eisenbart J, Joseph J, Kalyanaraman B, Chandel NS. Mitochondrial complex III ROS regulate adipocyte differentiation. Cell Metab. 2011; 14:537–544. [PubMed: 21982713]

55. Mandal S, Lindgren AG, Srivastava AS, Clark AT, Banerjee U. Mitochondrial function controls proliferation and early differentiation potential of embryonic stem cells. Stem Cells. 2011; 29:486–495. [PubMed: 21425411]

56. Ryall JG. Metabolic reprogramming as a novel regulator of skeletal muscle development and regeneration. FEBS J. 2013; 280:4004–4013. [PubMed: 23402377]

57. Williamson DL, Butler DC, Alway SE. AMPK inhibits myoblast differentiation through a PGC-1alpha-dependent mechanism. Am J Physiol Endocrinol Metab. 2009; 297:E304–314. [PubMed: 19491292]

58. Fulco M, Schiltz RL, Iezzi S, King MT, Zhao P, Kashiwaya Y, Hoffman E, Veech RL, Sartorelli V. Sir2 regulates skeletal muscle differentiation as a potential sensor of the redox state. Mol Cell. 2003; 12:51–62. [PubMed: 12887892]

Highlights

- A CRISPR-generated stable tafazzin knockout myoblast cell line has been constructed.

- Tafazzin knockout cells exhibit mitochondrial deficits.

- Tafazzin knockout cells are consistent with other models of Barth syndrome.

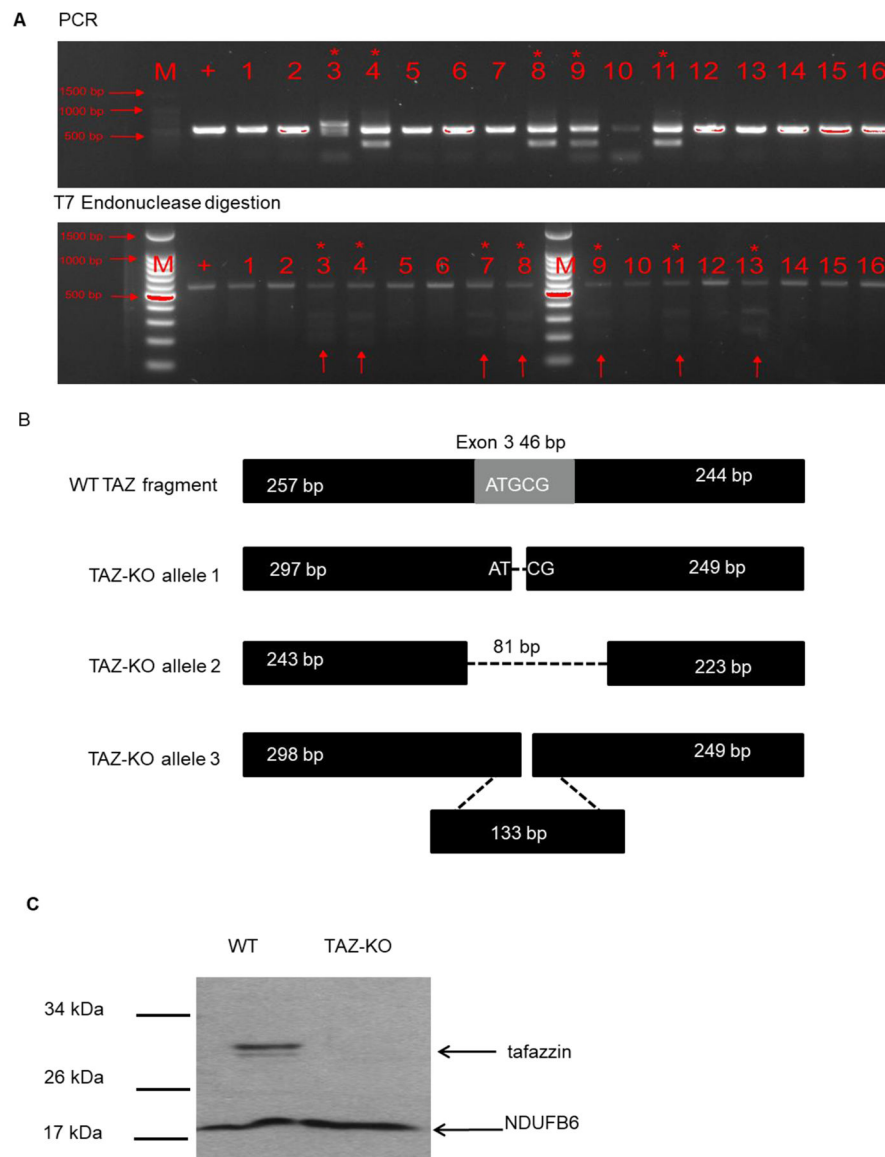- Tafazzin-deficiency was associated with impairment of myocyte differentiation.

Fig. 1. The construction of TAZ-KO C2C12 cells

Mouse C2C12 myoblast cells were transfected with CRISPR plasmid targeting the tafazzin gene. (A) Genomic TAZ is altered in TAZ-KO cells. Cells were selected in puromycin-containing DMEM with 10% FBS. The knockout strain was identified by PCR using the 547 bp region of the tafazzin gene targeted by the Cas9 gRNA followed by T7 endonuclease digestion. (B) TAZ alleles were identified by Sanger sequencing as described in Materials and Methods. (C) Tafazzin protein was not detectable in TAZ-KO cells. Cells were grown in DMEM with 10% FBS, harvested, and lysed for protein extraction. 30 μg of total cell extract from each sample were subjected to Western blot analysis using 10% polyacrylamide gels. The mitochondrial protein NDUFB6 was used as a loading control.
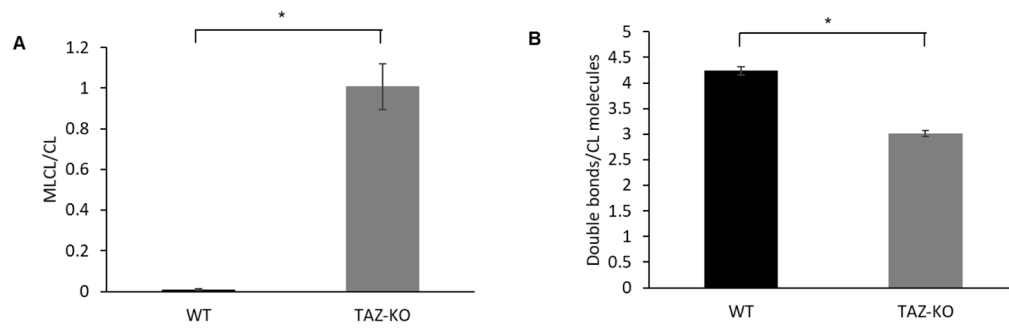
Fig. 2. CL profile of TAZ-KO cells

(A) MLCL/CL ratio of TAZ-KO cells was increased compared to WT controls. WT and TAZ-KO cells grown in DMEM to confluence were extracted for CL and MLCL content analysis by MALDI-TOF mass spectrometry. (B) CL saturation of TAZ-KO cells is increased, consistent with defective CL remodeling. (Data from at least three biological replicates were used for statistical comparisons, $p < 0.05$).
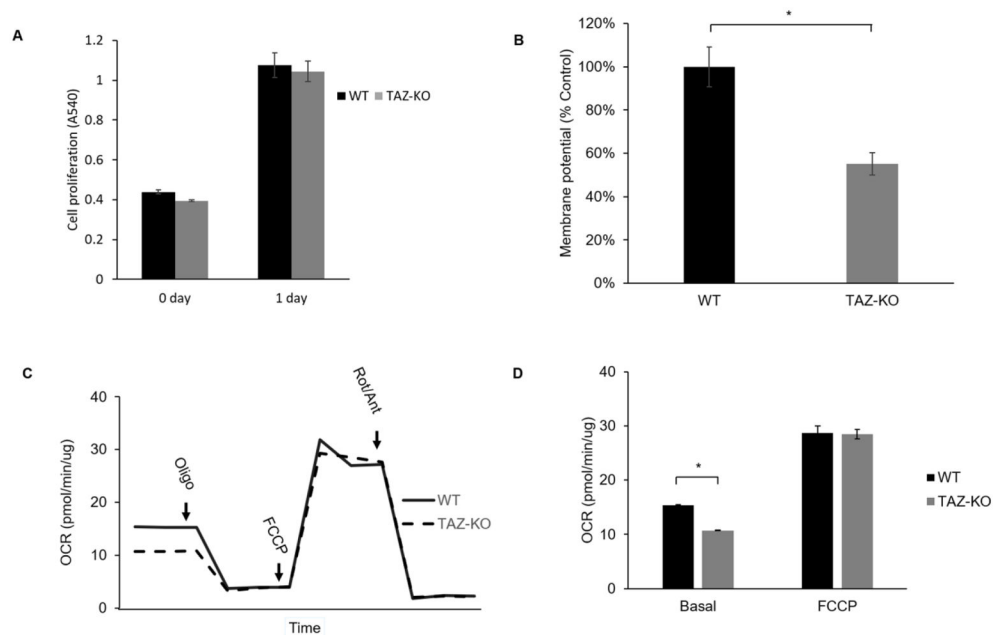
Fig. 3. Mitochondrial function is decreased in TAZ-KO cells
(A) C2C12 myoblast proliferation was not affected by tafazzin deficiency. WT and TAZ-KO cell proliferation in DMEM media with 10% FBS was measured using the MTT assay. (B) Mitochondrial membrane potential is significantly reduced in TAZ-KO cells. Membrane potential of growing WT and TAZ-KO cells was determined by fluorescence quantification of the ψ dependent dye TMRM. (Data from at least three biological replicates were used for statistical comparisons, p<0.05). (C–D) Oxygen consumption was measured in intact cells using a Seahorse analyzer. While maximal respiratory capacity was not affected by tafazzin deficiency, basal mitochondrial respiration was significantly decreased in TAZ-KO compared to control cells (p<0.05).
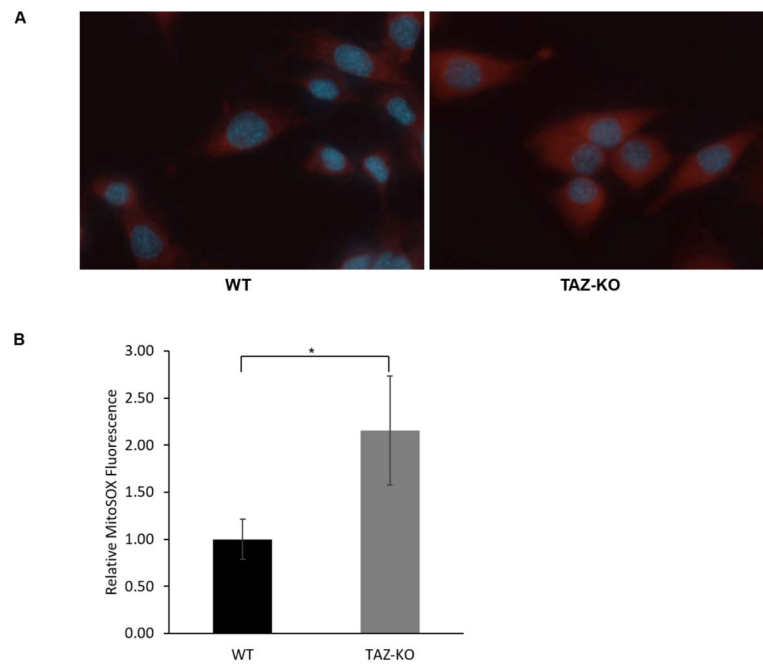
Fig. 4. Mitochondrial ROS production is increased in TAZ-KO cells

(A) An increase in mitochondrial ROS was observed in TAZ-KO cells. ROS production was measured via MitoSOX fluorescence using a Z1 AxioObserver inverted fluorescence microscope equipped with an AxioVision MRm camera (Zeiss). (B) Quantitative assessment of MitoSOX fluorescence was performed in all cells within five randomly selected fields of view from three biological replicates using fluorescence density analysis with ZenPro software (Zeiss). (Data from at least three biological replicates were used for statistical comparisons, $p < 0.05$).
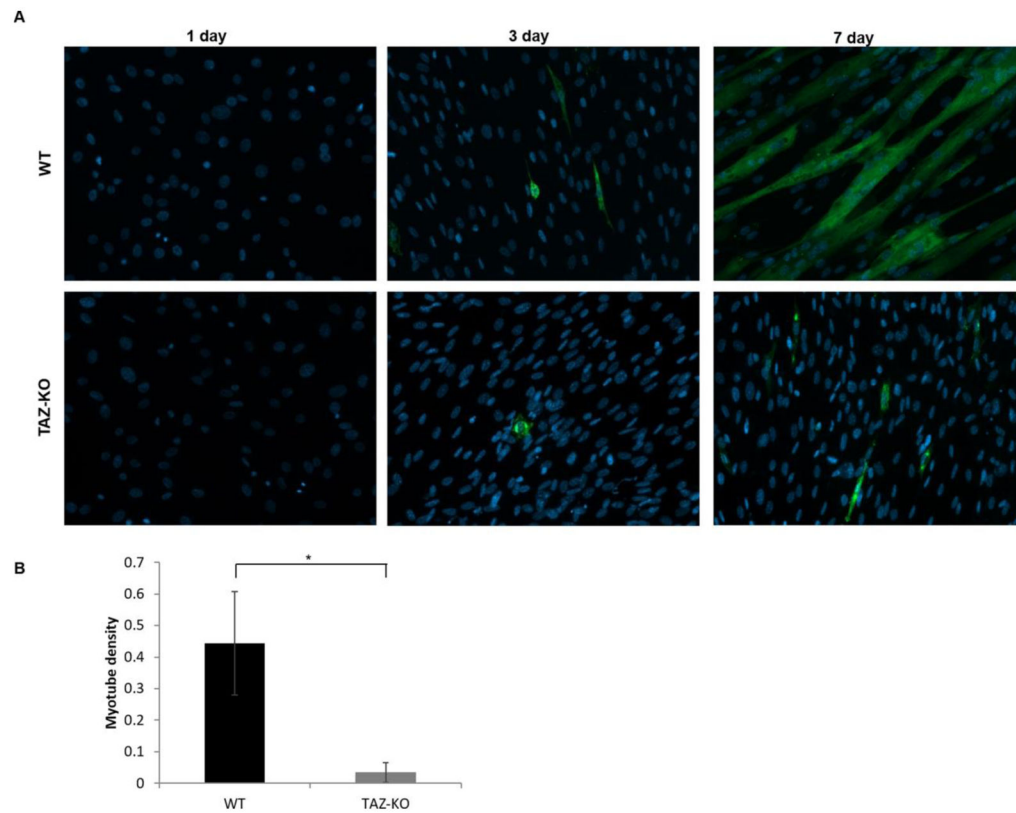
Fig. 5. Myogenic differentiation is reduced in TAZ-KO cells

(A) Myogenic differentiation was initiated in cells reaching confluence by switching the cells to DMEM medium containing 2% horse serum. Cells were cultured for 1, 3, or 7 days. Antibody detection of skeletal muscle contractile protein myosin heavy chain (MHC) was used for immunofluorescent staining of differentiated myotubes. (B) Myotube density was quantified via morphometric analysis using ZenPro software (Zeiss). MHC-positive myotubes were manually traced, and the myotube density was calculated by dividing the area occupied by MHC-positive myotubes by the total area of the field of view (Data from at least three biological replicates were used for statistical comparisons, p<0.05).
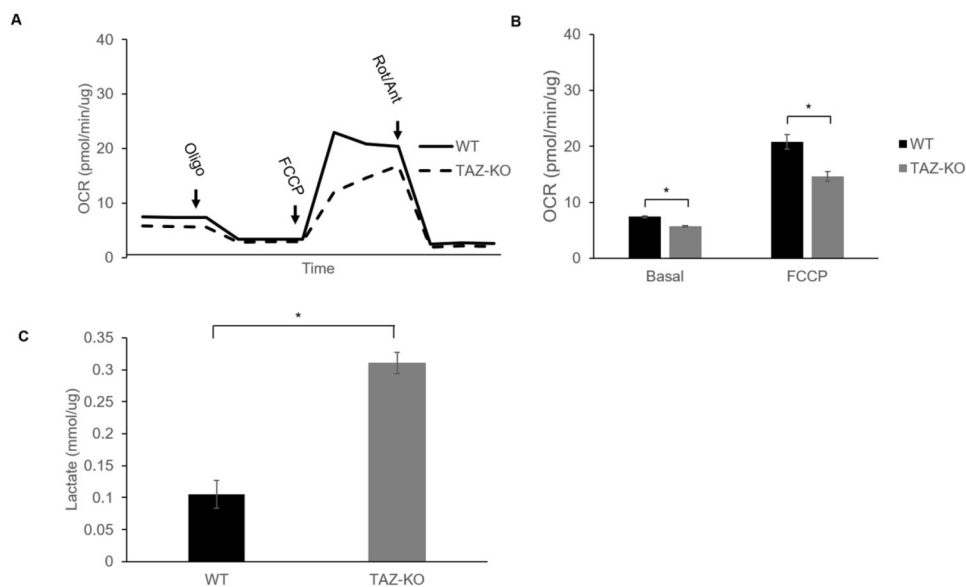
Fig. 6. Glycolytic metabolism is increased in TAZ-KO cells grown under differentiation conditions

(A–B) Basal mitochondrial respiration and maximal respiratory capacity are decreased in TAZ-KO cells compared to control cells following exposure to differentiation media for 7 days. Oxygen consumption was measured in intact cells using a Seahorse analyzer (Agilent, Santa Clara, CA). (C) An increase in lactate production was observed in TAZ-KO cells compared to control cells following exposure to differentiation media for 7 days. Lactate was measured with a kit (Pointe Scientific, Inc. Canton, MI) and was normalized to total protein. (Data from at least three biological replicates were used for statistical comparisons, $p<0.05$).